J Nanostruct 15(4): 1888-1899, Autumn 2025

RESEARCH PAPER

Synthesis and Characterization of Co_3O_4-Graphene Nanocomposites via Pulsed Laser Ablation in Liquids: Insights into Optical, Structural, and Morphological Properties

Ghufran Sabbar, Wasan M. Mohammed, Amer Al-Nafiey*

Department of Laser Physics, College of Science for Women, University of Babylon, Babylon, Iraq

ARTICLE INFO

Article History:
Received 10 June 2025
Accepted 17 September 2025
Published 01 October 2025

Keywords:
Co_3O_4-Graphene Nanocomposites
Energy Band Gap
Optical Properties
Pulsed Laser Ablation in Liquids (PLAL)
X-Ray Diffraction (XRD)

ABSTRACT

This study investigates the synthesis and characterization of cobalt oxide (Co_3O_4), graphene, and their nanocomposites (Co_3O_4-graphene) using pulsed laser ablation in liquids (PLAL). The nanomaterials were prepared by ablating solid targets of Co_3O_4 and graphene in deionized water under varying laser pulse conditions (300, 500, and 1000 pulses). UV-Vis spectroscopy revealed characteristic absorption edges and tunable energy gaps, with direct band gaps ranging from 1.5 eV to 2.0 eV and indirect band gaps from 2.25 eV to 2.65 eV, highlighting the influence of graphene incorporation on electronic properties. X-ray diffraction (XRD) analysis confirmed the crystalline nature of the materials, with average crystallite sizes of 1.53 nm for Co_3O_4 and 1.72 nm for graphene. Scanning electron microscopy (SEM) and atomic force microscopy (AFM) demonstrated spherical nanostructures with homogeneous distributions and reduced surface roughness in composite films. These findings underscore the potential of Co_3O_4-graphene nanocomposites for applications in optoelectronics, gas sensing, and energy-related technologies. The PLAL method proved to be an effective and versatile technique for tailoring the properties of nanomaterials with precision.

How to cite this article
Sabbar G., Mohammed W., Al-Nafiey A. Synthesis and Characterization of Co_3O_4-Graphene Nanocomposites via Pulsed Laser Ablation in Liquids: Insights into Optical, Structural, and Morphological Properties. J Nanostruct, 2025; 15(4):1888-1899. DOI: 10.22052/JNS.2025.04.036

INTRODUCTION

Nanotechnology has experienced remarkable advancements in recent decades, providing innovative tools and solutions across diverse fields. A defining feature of nanotechnology is its focus on materials at the nanometer scale—typically ranging from 1 to 100 nanometers. These nanomaterials have found extensive applications in medicine, industry, electronics, and environmental science, demonstrating exceptional efficacy in areas such as gas sensing. Examples of widely studied nanomaterials include metals like zinc, copper, gold, silver, and titanium, as well as oxides such as silver oxide, titanium oxide, zinc oxide, silicon oxide, cobalt oxide, and graphene oxide. Additionally, novel materials like nano-carbon and polymers have gained attention due to their unique properties [1]. These materials benefit from synergistic interactions between filler particles, further enhancing their performance [2].

Nanomaterials are classified based on their shape, size, and dimensionality into several categories, including nanoparticles, nanocrystals, nanotubes, nanofibers, and nanosheets. Their

* *Corresponding Author Email: ghufransabbar1@gmail.com*

properties are highly dependent on their size, shape, and chemical composition, making them distinct from bulk materials [3]. These unique characteristics encompass electromechanical, optical, chemical, and thermal properties, which have sparked significant interest in both scientific research and technological applications [4].

Based on their dimensional characteristics, nanomaterials can be categorized as follows: Zero-Dimensional (0D) Nanomaterials: These materials have all three dimensions at the nanoscale and include nanoparticles such as nanospheres, quantum dots, and metallic nanoparticles [5]. One-Dimensional (1D) Nanomaterials: These materials have one dimension at the nanoscale and include nanotubes, nanofibers, nanowires, carbon nanofibers, and quantum wires [6]. Two-Dimensional (2D) Nanomaterials: These materials have two dimensions at the nanoscale and include graphene sheets, nanosheets, and membranes [7]. The production of nanomaterials generally follows two fundamental approaches: the top-down approach and the bottom-up approach. Top-Down Approach: In this method, larger materials are broken down into smaller components using techniques such as mechanical milling, laser engraving, and chemical etching [8]. Bottom-Up Approach: This method involves assembling nanomaterials atom by atom or molecule by molecule. Techniques include self-assembly, surface chemistry, and chemical vapor deposition. While this approach allows for precise control over size and structure, it often requires advanced equipment and specific conditions [10]. In both approaches, the final properties of nanomaterials can be tailored by controlling the chemical and physical processes involved in their synthesis. Parameters such as size, shape, composition, structure, and surface properties can be adjusted to achieve desired functionalities. These tunable properties make nanomaterials invaluable for applications in electronics, medicine, energy, environmental remediation, and the development of ultra-strong materials [11]. Nanomaterials can be synthesized using either chemical or physical methods.

In this study, we employ pulsed laser ablation in liquids (PLAL) as a straightforward and safe physical method for producing nanomaterials. PLAL has emerged as a promising technique for synthesizing nanoparticles by ablating solid targets in liquid environments. Over the past two decades, laser ablation of solid materials—whether in gases, vacuums, or liquids—has been extensively investigated [11, 12]. This method has garnered significant attention due to its ability to produce nanoparticles with controlled properties. The process relies on laser parameters such as pulse duration, number of pulses, energy, wavelength, target material properties, and the surrounding medium, all of which influence the amount of material removed and the resulting nanoparticle characteristics [13].

MATERIALS AND METHODS

Materials

The target materials for this study included graphene plates with a purity greater than 99.9% and cobalt oxide (Co_3O_4) powder with a purity of 99.99%, both obtained from Sigma-Aldrich.

Preparation of Nano-solutions

Cobalt oxide was compressed into a disc using a hydraulic press, applying a pressure of approximately 7 tons to 5 grams of cobalt oxide powder. Nano cobalt oxide and graphene solutions were prepared via pulsed laser ablation (PLA) in a glass beaker containing 5 mL of deionized water. Pure cobalt and graphene plates were exposed to 300, 500,1000 laser pulses from a Q-switched Nd laser, operating at a wavelength of 1064 nm, a pulse width of 10 ns, a repetition rate of 4 Hz, and an energy of 140 mJ. The laser beam was focused perpendicularly onto the target material submerged in water, producing colloidal nano cobalt oxide and graphene solutions.

Fig. 1 illustrates the experimental arrangement for synthesizing graphene (G), cobalt oxide nanoparticles (Co_3O_4 NPs), and graphene-cobalt oxide nanocomposites (G-Co_3O_4 NPs) using PLA in deionized water.

A graphite plate was immersed in 5 mL of deionized water and subjected to 300, 500, and 1000 pulses from the Q-switched Nd laser under the aforementioned conditions. The process generated a graphene colloid (G) dispersed in water.

After removing the graphite plate, a cobalt plate replaced it in the beaker and underwent the same laser treatment. The process formed a cobalt oxide nanoparticle colloid (Co_3O_4 NPs) in the graphene solution. So, graphene-cobalt oxide nanocomposites (G-Co_3O_4 NPs) were synthesized.

Both graphene (G1000) and cobalt oxide (Co_3O_4

1000) solutions were produced individually under identical laser conditions.

Thin Film Preparation

The prepared nano-solutions were used to create thin films on 2 × 2 cm² glass substrates, which were thoroughly cleaned beforehand. A drop-casting method was applied to form films of cobalt oxide, graphene, and graphene-cobalt oxide nanocomposites individually. The films were

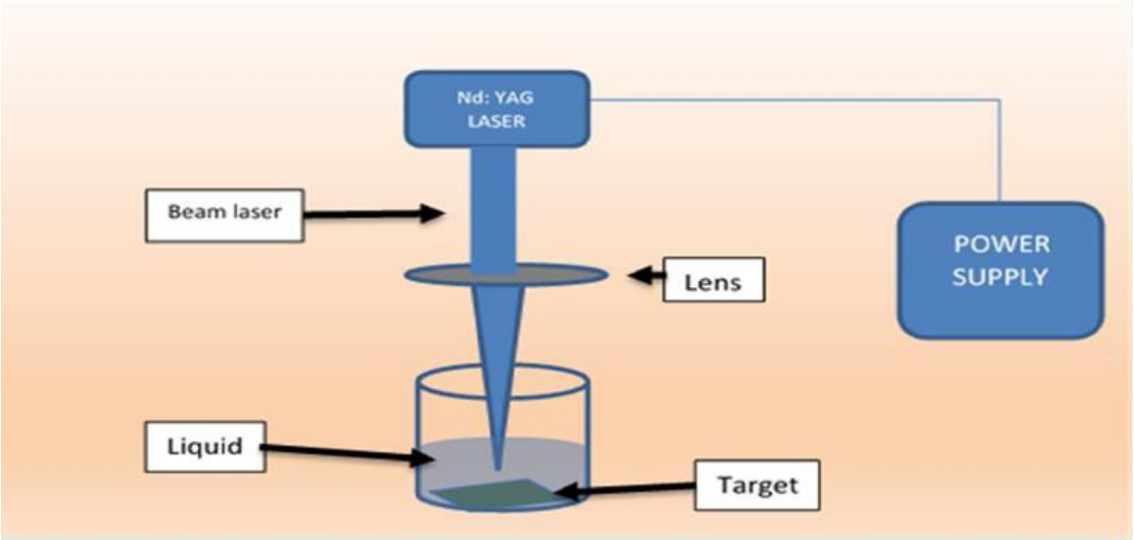

Fig. 1. Laser ablation in liquids.

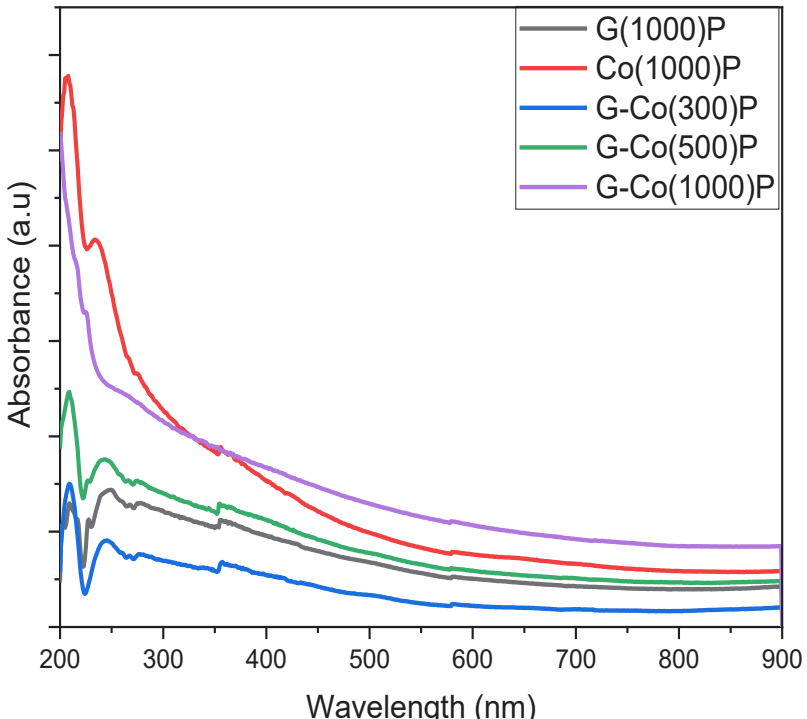

Fig. 2. UV–vis spectra of the Co_3O_4, graphene, Co_3O_4-graphene (1000), Co_3O_4-graphene (500), and Co_3O_4-graphene (300).

annealed at 400°C for one hour.

Characterization

Field Emission Scanning Electron Microscopy (FE-SEM, F50, FEI) was employed to analyze the sample morphology. The crystal structure and average crystallite size were determined using X-ray diffraction (XRD, SHIMADZU 6000, Japan), with scans performed over a 2θ range of 10° to 70°.

RESULTS AND DISCUSSION

Optical properties

UV-Vis absorption

The UV-Vis spectrum of graphene shows an absorption edge at 215 nm, with a peak centered at 210 nm. For the composite material G-Co (500), the position of the absorption peak remains unchanged; however, the intensity of the absorption undergoes a noticeable shift. Specifically, the absorption intensity of cobalt (Co) increases, while the intensity of graphene (G) decreases in the composite material (G-Co). This behavior can be attributed to the formation of a core-shell structure, where cobalt nanoparticles are encapsulated by graphene layers.

In contrast, for the composite G-Co (1000), the absorption edge shifts to 200 nm, accompanied by a significant increase in absorption intensity. These changes suggest a stronger interaction between cobalt and graphene in the G-Co (1000) composite compared to G-Co (500). The observed trends are illustrated in Fig. 2.

Absorption coefficient

The Fig. 3 illustrates the absorption coefficient of Co_3O_4, graphene, and their composites across a range of wavelengths. Co_3O_4exhibits low absorption, while graphene demonstrates high and consistent absorption across the spectrum. The Co_3O_4-graphene composites show intermediate absorption values, higher than

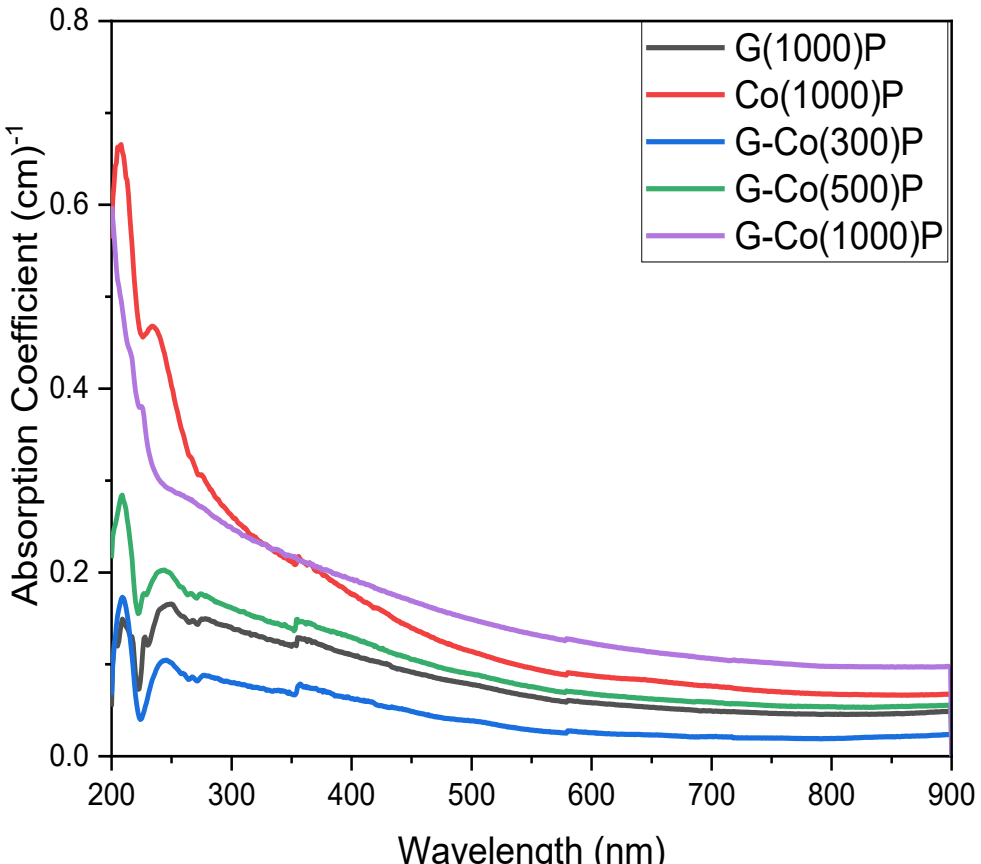

Fig. 3. shows the absorption coefficient at Co_3O_4, graphene, Co_3O_4-graphene (1000), Co_3O_4-graphene (500), and Co_3O_4-graphene (300).

Co_3O_4but lower than graphene, indicating that the presence of graphene enhances the composite's light absorption. Different variations of the composite (G-Co (300)P, G-Co(500)P, G-Co(1000) P) suggest that the absorption properties can be tuned by adjusting the ratio or structure of the materials. These tunable absorption properties make Co_3O_4-graphene composites promising for applications like photodetectors, solar cells, and optical coatings. The absorption coefficient values are shown in the Table 1.

The Table 1 presents the absorption coefficients of Co_3O_4, graphene, and their composites at specific near-ultraviolet wavelengths. Co_3O_4 exhibits a higher absorption coefficient than graphene at these wavelengths. The Co_3O_4-graphene composites demonstrate absorption values between those of the individual components, indicating that the combination influences light absorption. Notably, the absorption coefficient of the composites appears to decrease as the numerical identifier in their label decreases (from 1000 to 300), suggesting that variations in the composite's composition or structure affect its

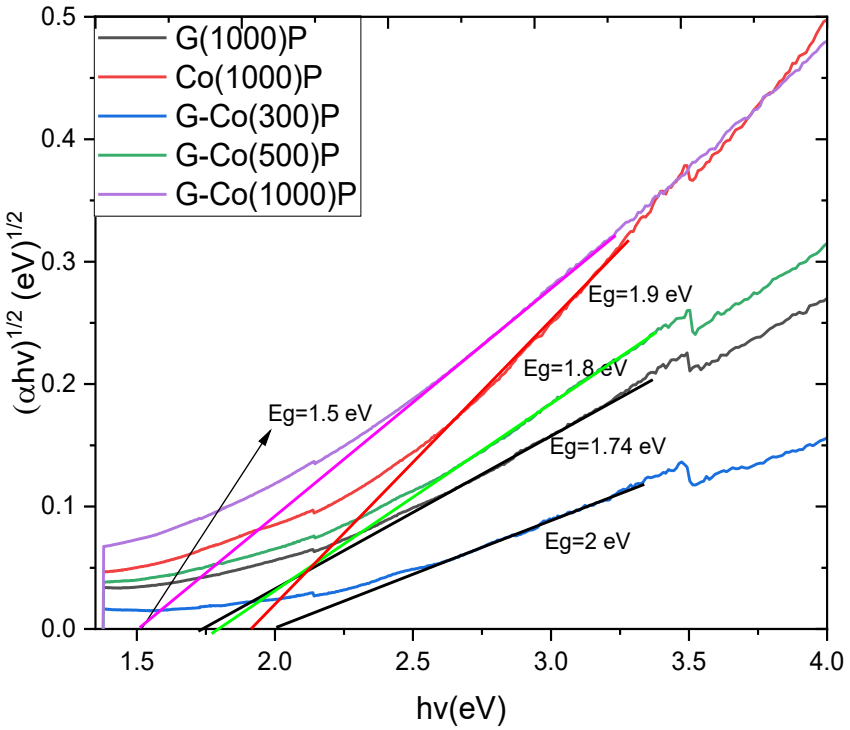

Fig. 4. Direct energy gap for Co_3O_4, graphene, Co_3O_4-graphene (1000), Co_3O_4-graphene (500), and Co_3O_4-graphene (300).

Table 1. The absorption coefficient for Co_3O_4, graphene, Co_3O_4-graphene (1000), Co_3O_4-graphene (500), and Co_3O_4-graphene (300).

Nanocomposites	Absorption coefficient(α) cm^{-1}	Wavelength (λ)(nm)	Ref. n
Co_3O_4 (1000)	0.65289	210	0.34706542
Graphene (1000)	0.13490	207	0.1383393
Co_3O_4-graphene (1000)	0.59850	200	0.31332
Co_3O_4-graphene (500)	0.27787	207	0.17649
Co_3O_4-graphene (300)	0.16769	211	0.14621

absorption properties. The refractive index for each material at the measured wavelength is also provided.

Energy Gaps

Fig. 4 presents Tauc plots for Co_3O_4, graphene, and their composites, revealing their direct band gap energies. Co_3O_4exhibits the largest band gap at approximately 2 eV, while graphene's band gap is around 1.8 eV. The Co_3O_4-graphene composites show band gap energies between these values, demonstrating that combining the materials modifies the electronic structure. Furthermore, variations in the composite's composition or structure, denoted by the numbers 1000, 500, and 300, appear to influence the band gap energy, suggesting the possibility of tuning this property. These results indicate that incorporating graphene into Co_3O_4 creates materials with adjustable band gaps.

While Fig. 5 presents Tauc plots assuming indirect band gap transitions for Co_3O_4, graphene, and their composites. The analysis reveals indirect band gap energies around 2.5 eV for Co_3O_4, 2.4 eV for graphene, and values ranging from 2.25 eV to 2.65 eV for the Co_3O_4-graphene composites. However, the validity of the indirect band gap assumption requires further investigation using complementary techniques, as the band gap values obtained here differ significantly from those calculated assuming direct transitions (Fig. 5). This discrepancy highlights the importance of correctly identifying the nature of the electronic transitions in these materials for accurate band gap determination.

The energy gaps (both direct and indirect) for Co_3O_4, graphene, and their composites (Co_3O_4-graphene) at varying *ratios* of graphene reveal distinct trends in electronic properties. For the direct energy gap (Table 2), Co_3O_4 (1000) exhibits a value of 1.9 eV, while the Co_3O_4-graphene (1000) composite shows a *reduced* gap of 1.5 eV, indicating enhanced interactions between Co_3O_4 and graphene at higher graphene content. Pure graphene (1000) has a direct energy gap of 1.74 eV, while the direct gaps of the composites range from 2.0 eV (300) down to 1.5 eV (1000). In contrast, the indirect energy gaps (Table 3) are *significantly* higher than their direct counterparts, with Co_3O_4 (1000) and graphene (1000) both showing 2.5 eV, while the indirect gaps of the composites are *reduced* from 2.65 eV (300) down to 2.25 eV

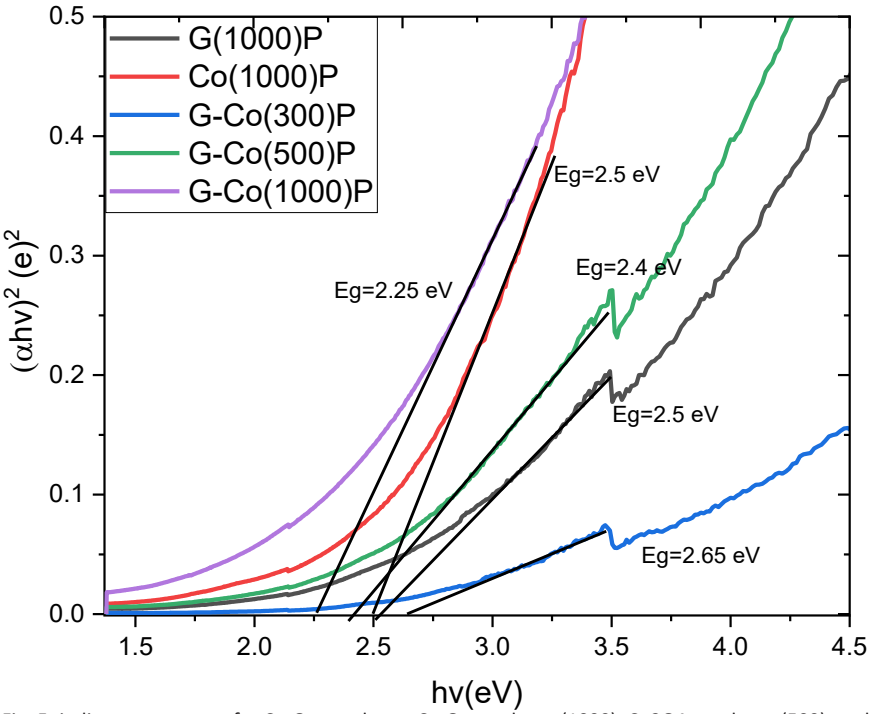

Fig. 5. indirect energy gap for Co_3O_4, graphene, Co_3O_4-graphene (1000), Co3O4-graphene (500), and Co3O4-graphene (300).

(1000), reflecting stronger quantum confinement effects. Notably, both direct and indirect energy gaps *decrease* with increasing graphene content, highlighting graphene's role in enhancing charge carrier interactions and *reducing* the energy gap, which underscores the potential of these composites for optoelectronic and energy-related applications.

Structural properties

X-Ray Diffraction (XRD)

Fig. 6 presents the X-ray diffraction (XRD) patterns of pure graphene, pure cobalt oxide, and G-Co_3O_4 NPs nanocomposite thin films, obtained for samples annealed at 400°C and scanned over a 2θ range of 10° to 70°.

* G 1000 (Graphene at 1000 pls): The black curve represents pure graphene prepared at a laser energy of 1000 pls. The broad peak around 2θ=26° is typical for graphene, corresponding to the (002) plane, indicating the presence of graphene sheets.

* Co 1000 (Cobalt Oxide at 1000 pls): The red curve represents pure cobalt oxide, showing distinct peaks around 2θ=31°, 37°, and 45°, which are characteristic of cobalt oxide phases such as CoO or Co_3O_4. These peaks confirm the crystalline nature of cobalt oxide in the sample.

* G-Co 300, 500, 1000 (Graphene-Cobalt Oxide Nanocomposite): The blue, light blue, and green curves correspond to graphene-cobalt oxide composites prepared at different laser pluses (300, 500, and 1000 pls). In these patterns, we can see peaks that likely correspond to both graphene (broad peak around 26°) and cobalt oxide (sharp peaks around 31°, 37°, and 45°). The variation in peak intensity with laser energy might indicate changes in crystallinity or relative composition in the composite.

In details, the XRD pattern of pure graphene exhibits a broad peak centered around 26°, corresponding to the (002) plane of graphitic carbon, which reflects its polycrystalline and turbostratic structure. For pure cobalt oxide, sharp diffraction peaks confirm the formation of crystalline Co_3O_4 with a cubic phase. Notable peaks at 37°, 38°, 47°, and 62° correspond to the (311), (222), (400), and (331) planes, respectively, verifying the well-defined crystalline nature of Co3 O4 as in report [14]. The data from JCPDS-76-1802 indicates that the sample had a polycrystalline structure, and all of the detected peaks may be attributed to it [15].

The XRD patterns of the G-Co_3O_4 NPs nanocomposites show combined peaks from both graphene and cobalt oxide, indicating successful integration of both components. The broad graphene peak at 26° remains visible, while sharp peaks from cobalt oxide are present, suggesting cobalt oxide nanoparticles are well-dispersed on

Table 2. Direct energy gap for Co_3O_4, graphene, Co_3O_4-graphene (1000), Co_3O_4-graphene (500), and Co_3O_4-graphene (300).

Nano material	Energy gap (ev)
Co_3O_4 (1000)	1.9
Graphene (1000)	1.74
Co_3O_4-graphene (300)	2
Co_3O_4-graphene (500)	1.8
Co_3O_4-graphene (1000)	1.5

Table 3. in Direct energy gap for Co3O4, graphene, Co_3O_4-graphene (1000), Co_3O_4-graphene (500), and Co_3O_4-graphene (300).

Nano material	Energy gap (ev)
Co_3O_4 (1000)	2.5
Graphene (1000)	2.5
Co_3O_4-graphene (300)	2.65
Co_3O_4-graphene (500)	2.4
Co_3O_4-graphene (1000)	2.25

the graphene matrix. The reduced intensity of the graphene peak in the composites suggests partial coverage of graphene layers by cobalt oxide nanoparticles [16], which may enhance interaction between the two materials. Additionally, a peak at 38° suggests the possible presence of Co(OH)2 [17] , hinting at slight hydroxylation during synthesis.

Crystallite sizes of different phases were calculated using the Scherrer equation [18], as summarized in Table 4. The results reveal nanocrystalline structures, with the Co_3O_4 phase exhibiting crystallite sizes ranging from 1.85 nm to 352.4 nm across different crystallographic planes, with an average crystallite size of 57.3 nm. The peak at 47.1° shows a very small FWHM, suggesting a larger crystallite size (352.4 nm) in that plane, potentially indicating a more perfect crystal. However, defects could also contribute to peak broadening. Additionally, the new CoO phase with a crystallite size of 1.53 nm suggests the presence of very fine CoO nanoparticles, which may affect the overall material properties. For graphene, the crystallite size of 1.72 nm is typical for reduced graphene oxide (rGO) and could influence the material's electrical properties and interactions with the other phases.

The dhkl values in this table represent the interplanar spacings of different crystallographic

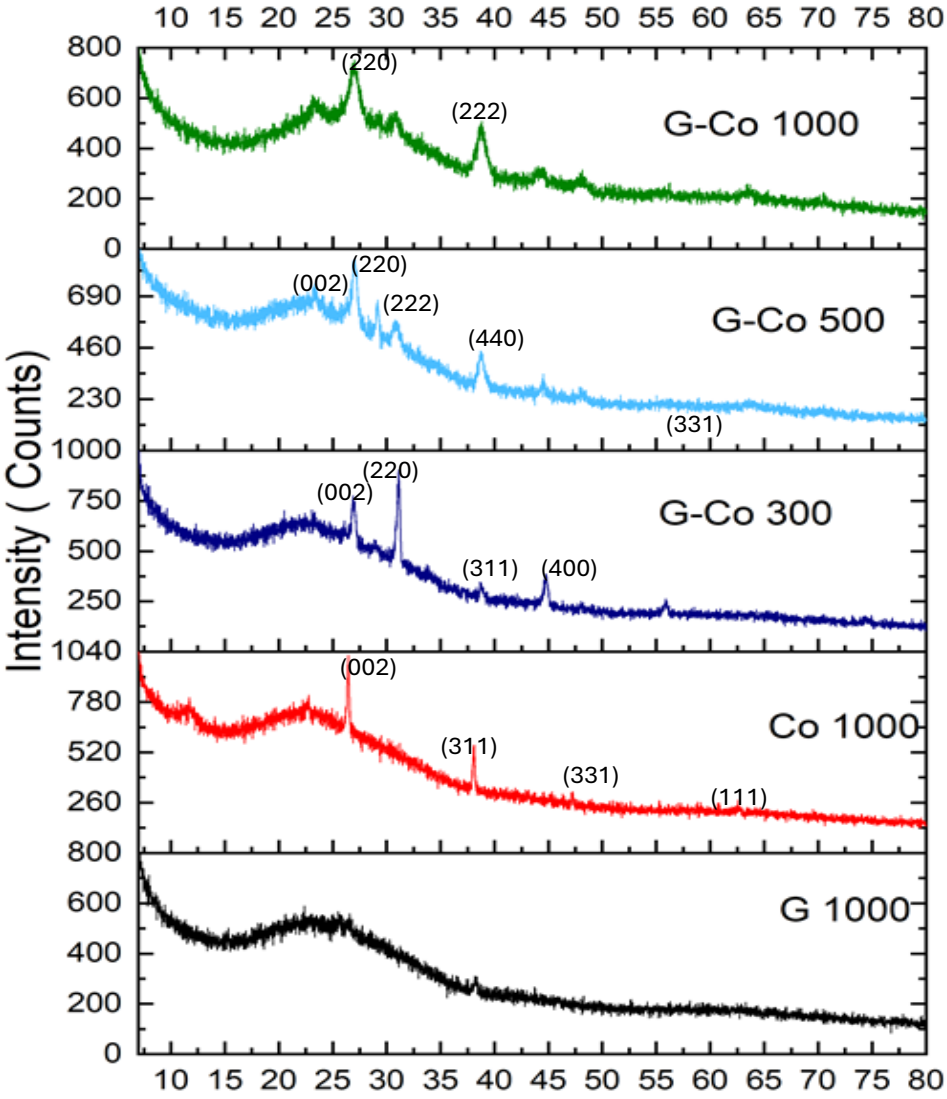

Fig. 6. XRD of pure cobalt oxide, graphene, and composited phase thin films on glass substrate.

planes in the Co_3O_4-CoO-graphene nanocomposites, providing insight into the structural characteristics of the material. The Co_3O_4 phase exhibits varying dhkl values across different planes (e.g., 3.86637 Å for (220), 3.37593 Å for (311), and 1.92645 Å for (440)), reflecting the different orientations and lattice arrangements in the oxide phase. The CoO phase, with a smaller dhkl value of 1.47689 Å (for the (111) plane), indicates a denser crystal structure and suggests the formation of CoO nanoparticles alongside Co_3O_4. The graphene phase is identified with a dhkl value of 3.30752 Å (for the (002) plane), typical for reduced graphene oxide, indicating a layered structure.

These nanocrystalline characteristics contribute to enhanced properties, with smaller crystallite sizes generally associated with improved crystallinity and interfacial interactions. The XRD analysis confirms the successful synthesis of rGO / Co_3O_4 nanocomposites, providing valuable insights into the material's phase composition, crystal structure, and particle size, which are crucial for its potential applications in photonics.

Scanning electron microscope (SEM)

Fig. 7 show the cobalt oxide, graphene, and composited phase thin films. The SEM image shows structures that resemble nanoscale ones. The nanostructure exhibits homogeneous distribution and alignment. The surface is covered in tiny granular particles companied with each other like shells are as shown in cobalt oxide image Fig. 7a. This figure indicate that the particles are extremely small, spherical, and have a size about (23.9-50.53) nm for cobalt. Fig. 7b the indicate the film has extremely small spherical particle, have a size about (25.35-34.77) nm for graphene. The micrographs of cobalt and graphene films have been formed from grains of nearly similar size and shape. Fig 7 c-f indicates that the morphology of composited films have been spherical flower-like nanostructure. The shape of the mixed composite thin film changed and the particle size of mixed composite thin film increased with increasing the pulses of laser. Show (36.51-51) nm for (G-Co 1000) composited sample, (38.4-42.41) nm for (G-Co 500) composited sample, (29.24-43.03) nm for (G-Co 300) composite samples. Where these results shows nanostructure appropriate for gas sensor and optoelectronic applications.

Atomic Force Microscope (AFM)

The images of AFM composite thin films are shown in Fig. 8. In the Co (1000) sample in Fig. 8, detailed surface structure details are highlighted, where fine spherical grains are formed, and this sample is characterized by small dimensions and low surface roughness. A study published in the "Materials Science" journal showed that the AFM results for Cobalt indicated that the surface roughness (Rq) ranges between (0.8 - 1.2) nm, which is similar to the results in Table 5 [19]. The G(1000) sample has dimensions very close to Co (1000) with low surface roughness. From Fig. 7, we observe that Graphene shows very slight variations due to the smoothness of its surface. The "Carbon" journal analyzed Graphene using AFM, where the surface roughness (Ra) was found to

Table 4. Comparison between the Exp. and Std. value of d_{hkl} for

2θ (Deg.)	FWHM (Deg.)	d_{hkl} (Å)	D (nm)	Phase	hkl
32.9839	3.6123	3.86637	13	Cub. Co3O4	(220)
37.3791	0.7004	3.37593	67	Cub. Co3O4	(311)
38.043	0.1552	2.36344	634	Cub. Co3O4	(222)
47.1381	0.0246	1.92645	30450	Cub. Co3O4	(440)
62.8749	6.0777	1.47689	8	CoO	(111)
26.9349	4.7456	3.30752	9	Graphene	(002)
30.9127	4.4478	2.89038	10	Cub. Co3O4	(220)
38.7288	1.1197	2.32315	60	Cub. Co3O4	(311)(222)
44.2239	1.2506	2.0464	45	Cub. Co3O4	(400)
48.0391	0.4	1.8924	129	Cub. Co3O4	(331)

range between (0.5 and 0.8) nm, which aligns with the results we obtained [20]. As for the composite samples of (Co-G), the morphological changes that occur when combining Cobalt and Graphene

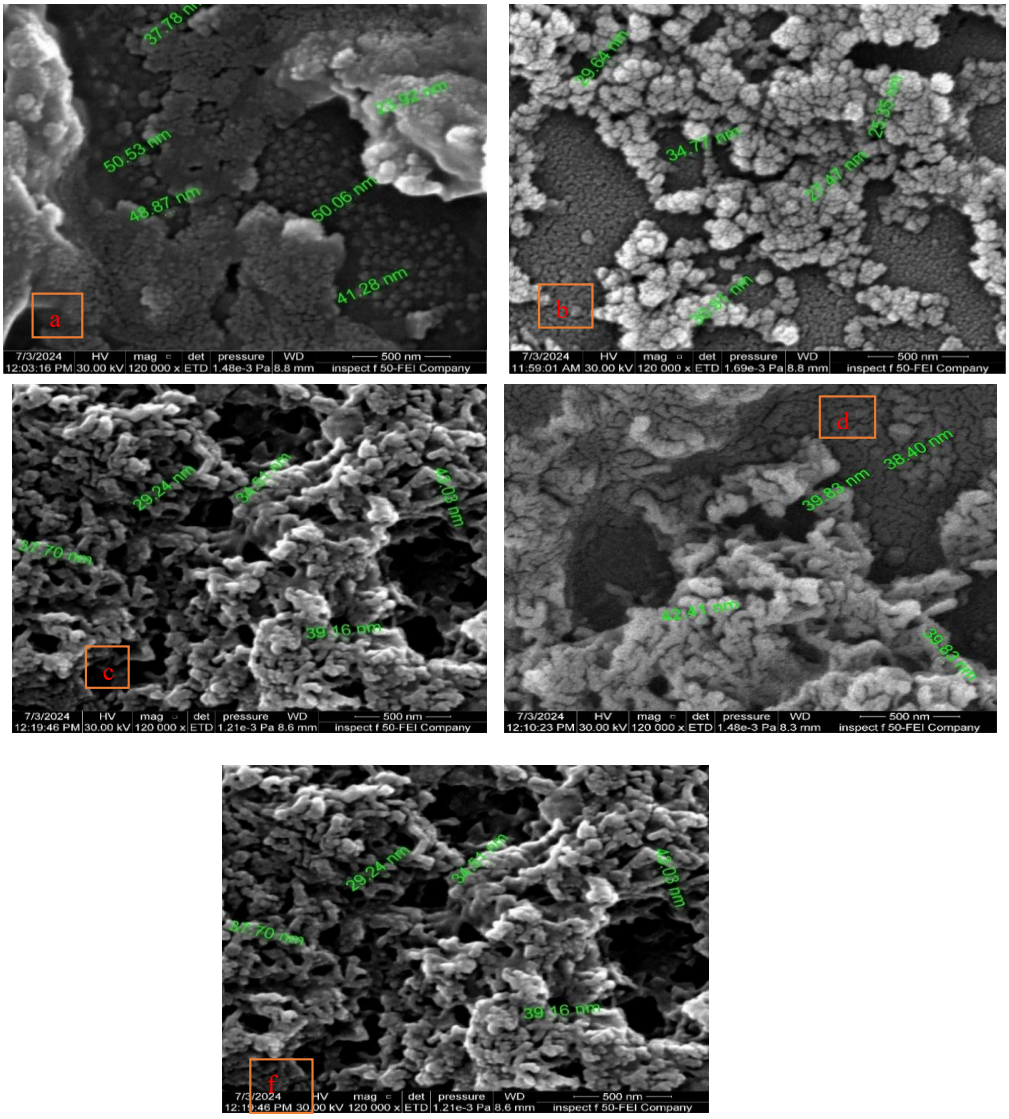

Fig. 7. The FESEM images of thin film deposited on glass substrate (a) Co_3O_4 (b) graphene (c) Co_3O_4-graphene (1000) (d) Co_3O_4-graphene (500). (f) Co_3O_4-graphene (300).

Table 5. The roughness (Ra), root mean square (Rq), and grain size (D).

Sample	Ra (nm)	Rq (nm)	D(nm)
$CO_{(1000)p}$	733.606×10^{-3}	909.007×10^{-3}	4.40829
$G_{(1000)p}$	711.508×10^{-3}	942.044×10^{-3}	4.6105
$G\text{-}CO_{(300)p}$	684.673×10^{-3}	960.994×10^{-3}	5.6291
$G\text{-}CO_{(500)p}$	612.626×10^{-3}	986.463×10^{-3}	8.5088
$G\text{-}CO_{(1000)p}$	1.50669	2.27140	13.9689

are highlighted, reflecting the nano-structure of the formed compound. The dimensions of the composites increase; surface roughness decreases with the increase in the number of pulses.

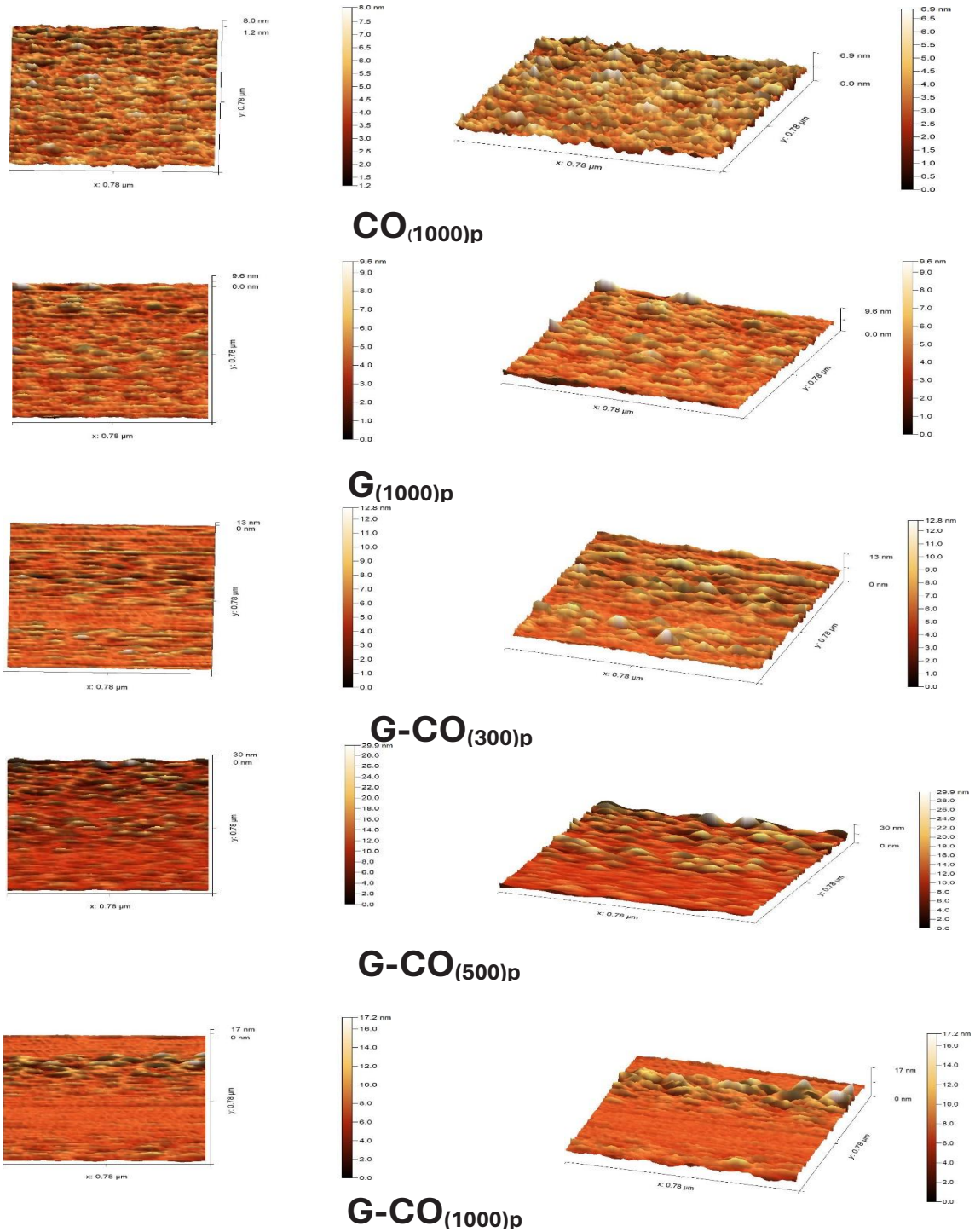

Fig. 8. AFM images of the (G-CO) prepared thin films.

CONCLUSION

This study successfully demonstrated the synthesis of Co_3O_4, graphene, and their nanocomposites using pulsed laser ablation in liquids (PLAL), highlighting its efficacy as a precise and tunable method for nanomaterial fabrication. The optical properties of the synthesized materials revealed tunable direct and indirect energy gaps, with values ranging from 1.5 eV to 2.65 eV, depending on the graphene concentration and composite structure. X-ray diffraction (XRD) confirmed the crystalline nature of the materials, while SEM and AFM analyses revealed uniform spherical nanostructures with controlled surface roughness, indicating strong interfacial interactions between Co_3O_4 and graphene. These structural and morphological characteristics make the nanocomposites highly suitable for applications in gas sensors, optoelectronics, and energy storage devices. Overall, the results emphasize the versatility of PLAL in producing high-quality nanomaterials with tailored properties, paving the way for advancements in diverse technological fields. Future work could explore the functional performance of these nanocomposites in real-world device applications to further validate their potential.

CONFLICT OF INTEREST

The authors declare that there is no conflict of interests regarding the publication of this manuscript.

REFERENCES

1. Aydn A, Sipahi H, Charehsaz M. Nanoparticles Toxicity and Their Routes of Exposures. Recent Advances in Novel Drug Carrier Systems: InTech; 2012.
2. Crosby AJ, Lee JY. Polymer Nanocomposites: The "Nano" Effect on Mechanical Properties. Polymer Reviews. 2007;47(2):217-229.
3. Manasreh O. Introduction to Nanomaterials and Devices: Wiley; 2011 2011/11/04.
4. Alarifi IM. Introduction, properties, and application of synthetic engineering nanomaterials. Synthetic Engineering Materials and Nanotechnology: Elsevier; 2022. p. 177-193.
5. Chi L. One-Dimensional Nanostructures. Principles and Applications. Herausgegeben von Tianyou Zhai und Jiannian Yao. Angew Chem. 2013;125(42):11144-11145.
6. Two-Dimensional Nanostructures for Energy-Related Applications: CRC Press; 2017 2017/03/27.
7. Chen L-C, Wu J-R. Graphene Applications in Optoelectronic Devices. Two-Dimensional Nanostructures for Energy-Related Applications: CRC Press; 2017. p. 99-118.
8. Enghag P. Encyclopedia of the Elements: Wiley; 2004 2004/07/27.
9. Weckenmann A. A Review of: "Precision Engineering, V. C. Venkatesh, S. Izman". Machining Science and Technology. 2009;13(2):282-283.
10. Biswas A, Bayer IS, Biris AS, Wang T, Dervishi E, Faupel F. Advances in top–down and bottom–up surface nanofabrication: Techniques, applications and future prospects. Advances in Colloid and Interface Science. 2012;170(1-2):2-27.
11. Nadimpalli NKV, Bandyopadhyaya R, Runkana V. Thermodynamic analysis of hydrothermal synthesis of nanoparticles. Fluid Phase Equilib. 2018;456:33-45.
12. Brown MS, Arnold CB. Fundamentals of Laser-Material Interaction and Application to Multiscale Surface Modification. Springer Series in Materials Science: Springer Berlin Heidelberg; 2010. p. 91-120.
13. Nafiujjaman M, Nurunnabi M. Graphene and 2D Materials for Phototherapy. Biomedical Applications of Graphene and 2D Nanomaterials: Elsevier; 2019. p. 105-117.
14. Şahan H, Göktepe H, Yıldız S, Çaymaz C, Patat Ş. A novel and green synthesis of mixed phase CoO@ Co_3O_4@C anode material for lithium ion batteries. Ionics. 2018;25(2):447-455.
15. Xu C, Wang X, Zhu J, Yang X, Lu L. Deposition of Co_3O_4nanoparticles onto exfoliated graphite oxide sheets. J Mater Chem. 2008;18(46):5625.
16. Moon IK, Lee J, Ruoff RS, Lee H. Reduced graphene oxide by chemical graphitization. Nature Communications. 2010;1(1).
17. Zhou XJ, Shi PH, Qin YF, Fan JC, Min YL, Yao WF. Synthesis of Co_3O_4/graphene composite catalysts through CTAB-assisted method for Orange II degradation by activation of peroxymonosulfate. Journal of Materials Science: Materials in Electronics. 2015;27(1):1020-1030.
18. Rusu DI, Rusu GG, Luca D. Structural Characteristics and Optical Properties of Thermally Oxidized Zinc Films. Acta Phys Pol, A. 2011;119(6):850-856.
19. Jafari A, Alam MH, Dastan D, Ziakhodadadian S, Shi Z, Garmestani H, et al. Statistical, morphological, and corrosion behavior of PECVD derived cobalt oxide thin films. Journal of Materials Science: Materials in Electronics. 2019;30(24):21185-21198.
20. Cambridge University Press, 1696-1712. Cambridge University Press 1696–1712: Cambridge University Press; 2016. p. 445-448.